Conclusions

Electrochemical, photochemical, fluorescence quantum yield, and excited singlet state lifetimes have been found to support the results of AM1 calculations, indicating a crossover between σ^* and π^* LUMO states when the aryl ring is naphthacene in some sulfonium salt derivatives. The preceding conclusions apply in general to other onium salts. Phosphonium salts would be expected to behave in a similar fashion to sulfonium salts, while ammonium and oxonium salts would be expected to show the σ^*/π^* crossover between naphthalene and anthracene.

Characterization of Pd-β-Cyclodextrin Colloids as Catalysts in the Photosensitized Reduction of Bicarbonate to Formate[†,1]

Itamar Willner* and Daniel Mandler

Contribution from the Department of Organic Chemistry, The Hebrew University of Jerusalem, Jerusalem 91904, Israel. *Received April 7, 1988*

Abstract: Photosensitized reduction of bicarbonate, HCO_3^-, to formate, HCO_2^-, proceeds in an aqueous system composed of deazariboflavin, dRFl (**1**), as photosensitizer, *N,N'*-dimethyl-4,4'-bipyridinium, MV^{2+}, as primary electron acceptor, sodium oxalate as sacrificial electron donor, and in the presence of a Pd colloid stabilized by β-cyclodextrin, Pd-β-CD. The process proceeds with a quantum efficiency, $\phi = 1.1$. Kinetic characterization of the Pd-β-CD catalyst activity reveals the presence of active sites for bicarbonate activation and reduction as well as catalytic sites for H_2 evolution. The HCO_3^- activation sites are specifically inhibited by thiols. The catalytic reduction of HCO_3^- to HCO_2^- and the respective inhibition processes exhibit enzyme-like kinetic properties. The Pd-β-CD colloid shows reversible activities and effects the reduction of MV^{2+} by formate. Kinetic characterization of the catalyzed reduction of HCO_3^- to HCO_2^- and the reverse oxidation of HCO_2^- provides a sequential mechanism for the reactions.

Photoreduction of CO_2, its hydrated form, carbonic acid, or its dissociated ions, bicarbonate and carbonate (eq 1), using visible

$$CO_2 + H_2O \rightleftharpoons H_2CO_3 \rightleftharpoons H^+ + HCO_3^- \rightleftharpoons 2H^+ + CO_3^{2-} \quad (1)$$

solar light is a challenging subject as a means of mimicking photosynthesis and of solar energy conversion and storage.[2-4] The standard redox potentials[5,6] for the reduction of carbon dioxide (at pH = 7) to C_1-carbon fuel products are given in eq 2-7 and

$$CO_2 + 2H^+ + 2e^- \rightarrow CO + H_2O \qquad E^\circ = -0.52\ V \quad (2)$$

$$CO_2 + 2H^+ + 2e^- \rightarrow HCO_2H \qquad E^\circ = -0.42\ V \quad (3)$$

$$CO_2 + 4H^+ + 4e^- \rightarrow HCHO + H_2O \qquad E^\circ = -0.48\ V \quad (4)$$

$$CO_2 + 6H^+ + 6e^- \rightarrow CH_3OH + H_2O \qquad E^\circ = -0.38\ V \quad (5)$$

$$CO_2 + 8H^+ + 8e^- \rightarrow CH_4 + 2H_2O \qquad E^\circ = -0.24\ V \quad (6)$$

$$2H^+ + 2e^- \rightarrow H_2 \qquad E^\circ = -0.41\ V \quad (7)$$

compared to that of H_2 evolution. It is evident that reduction of CO_2 in aqueous solutions to several C_1 products is thermodynamically favored over H_2 evolution. Nevertheless, reduction of CO_2 is encountered with severe kinetic difficulties, and extensive efforts are directed toward the activation of CO_2, bicarbonate, and carbonate by transition-metal complexes[7,8] or heterogeneous metal surfaces.[9,10]

Reduction of carbon dioxide could basically be accomplished through various pathways. These include hydrogenation,[11] insertion into transition-metal hydride complexes,[12] carbanion nucleophilic attack,[13] or by electron transfer followed by protonation.[14] The methanation process exemplifies an extensively explored hydrogenation of CO_2 to methane, a process that usually proceeds at elevated temperatures and high pressures.[15] Insertion of CO_2 into various transition-metal hydrides to form the formate ligand was observed.[16] Electrocatalyzed reduction of CO_2 was observed in the presence of various transition-metal complexes, i.e., Ni^{2+}- or Co^{2+}-cyclams,[17] metal porphyrins or phthalocyanins,[18] and iron-sulfur clusters,[19] or by using Ru or Cu metal catalysts as electrodes.[20] Hydrogenation of bicarbonate using

[†] Dedicated to the memory of Professor David Ginsburg.

(1) Mandler, D.; Willner, I. *J. Am. Chem. Soc.* **1987**, *109*, 7884.
(2) Inoue, S. In *Organic and Bioorganic Chemistry of Carbon Dioxide*; Inoue, S.; Yamazaki, N., Eds.; Kodansha Ltd.: Tokyo, Wiley: New York, 1982. p 253.
(3) Ziessel, R. *Nouv. J. Chim.* **1983**, *7*, 613.
(4) Åkermark, B. In *Solar Energy—Photochemical Conversion and Storage*; Claesson, S., Engstrom, L., Eds.; National Swedish Board for Energy Source Development: Stockholm, Sweden 1977.
(5) Latimer, W. M. *The Oxidation States of the Elements and their Potentials in Aqueous Solutions*, 2nd ed.; Prentice Hall: New York, 1952.
(6) Bard, A. J., Ed. *Encyclopedia of Electrochemistry of the Elements*; Dekker, New York, 1976.
(7) (a) Darensbourg, D. J.; Kudaroski, R. A. *Adv. Organomet. Chem.* **1983**, *22*, 129. (b) Palmer, D. A.; Eldvik, R. V. *Chem. Rev.* **1983**, *83*, 651. (c) Eisenberg, R.; Hendriksen, D. E. *Adv. Catal.* **1979**, *28*, 119.
(8) (a) Volpin, M. E.; Kolomnikov, I. S. *Pure Appl. Chem.* **1973**, *33*, 567. (b) Inoue, S. *Rev. Inorg. Chem.* **1984**, *6*, 291. (c) Ibers, J. A. *Chem. Soc. Rev.* **1982**, *11*, 57.
(9) (a) Solymosi, F.; Erdohelyi, A.; Lancz, M. *J. Catal.* **1985**, *95*, 567. (b) Solymosi, F.; Erdohelyi, A. *J. Mol. Catal.* **1980**, *8*, 471.
(10) Klier, K. *Adv. Catal.* **1982**, *31*, 243.
(11) Denise, B.; Sneeden, R. P. A. *CHEMTECH* **1982**, 108.
(12) Sneeden, R. P. A. *Compr. Organomet. Chem.* **1982**, *8*, 225.
(13) Haruki, E. F. in ref 2, pp 5-78.
(14) (a) Russel, P. G.; Kovac, N.; Srinivasan, S.; Steinberg, M. *J. Electrochem. Soc.* **1977**, *124*, 1329. (b) Amatore, C.; Saveant, J.-M. *J. Am. Chem. Soc.* **1981**, *103*, 5021.
(15) Solymosi, F.; Erdohelyi, A.; Kocsis, M. *J. Chem. Soc., Faraday Trans. 1* **1981**, *77*, 1003.
(16) Inoue, Y.; Izumida, H.; Sasaki, Y.; Hashimoto, H. *Chem. Lett.* **1976**, 863.
(17) (a) Fisher, B.; Eisenberg, R. *J. Am. Chem. Soc.* **1980**, *102*, 7361. (b) Beley, M.; Collin, J.-P.; Ruppert, R.; Sauvage, J. P. *J. Chem. Soc., Chem. Commun.* **1984**, 1315. (c) Beley, M.; Collin, J.-P.; Ruppert, R.; Sauvage, J.-P. *J. Am. Chem. Soc.* **1986**, *108*, 7461. (d) Petit, J.-P.; Chartier, P. *Nouv. J. Chim.* **1987**, *11*, 751.
(18) (a) Hiratsuka, K.; Takahashi, K.; Sasaki, H.; Toshima, S. *Chem. Lett.* **1977**, 1137; Ibid. **1979**, 305. (b) Kapusta, S.; Hackerman, N. *J. Electrochem. Soc.* **1984**, 1511. (c) Liber, C. M.; Lewis, N. S. *J. Am. Chem. Soc.* **1984**, *106*, 5033.
(19) Tezuka, M; Yajima, T.; Tsuchiya, A. *J. Am. Chem. Soc.* **1982**, *104*, 6834.
(20) (a) Frese, K. W., Jr.; Leach, S. *J. Electrochem. Soc.* **1985**, 259. (b) Summers, D. P.; Frese, K. W., Jr. *Langmuir* **1988**, *4*, 51.

0002-7863/89/1511-1330$01.50/0

supported Pd catalysts has been the subject of several reports.[21,22] Wrighton et al. have examined the hydrogenation[22] and electroreduction[23] of bicarbonate in the presence of supported Pd catalysts. In these processes effective formate production was accomplished at room temperature and close to the thermodynamic potential. Photoreduction of CO_2 has been reported in photochemical assemblies,[24-26] in the presence of semiconductor powders[27] or electrodes,[28] and in photosystems that include the enzyme formate dehydrogenase as biocatalyst.[29] In general, the reported photosystems of CO_2 reduction proceed with poor or unspecified quantum efficiencies. Photoreduction of CO_2 to carbon monoxide has been accomplished in aqueous media by using Co(II), Co(II)-bipyridine complexes, or Re(I)(bpy)$(CO)_3$X as homogeneous catalysts.[24,30] Photoreduction of CO_2 to formate has been reported in assemblies that included $Ru(bpy)_3^{2+}$ as photosensitizer and $Ru(bpy)_2L_2^{2+}$ as catalyst.[25,31] Recently, we have shown that heterogeneous Pd colloid stabilized by β-cyclodextrin, β-CD, catalyzes the photoreduction of bicarbonate to formate.[1] Photosensitized reduction of CO_2 to methane has been accomplished in microheterogeneous systems that include Ru or Os as heterogeneous catalysts.[24] Photoelectrochemical reduction of carbon dioxide to mixtures of C_1 products has been reported with semiconductor electrodes,[28] i.e., GaP or GaAs, or powder suspension[27] such as $SrTiO_3$. Nevertheless, these processes are inefficient. In the photosystems for CO_2 reduction that include heterogeneous metal colloids or homogeneous catalysts that operate through metal hydride species, H_2 evolution accompanies the CO_2 reduction process in aqueous media and the H_2 formation predominates in its effectiveness.

Here we report on the characterization of the catalytic activity of Pd-β-cyclodextrin colloids, Pd-β-CD, in the reduction of CO_2/HCO_3^- using *N,N'*-dimethyl-4,4'-bipyridinium radical, $MV^{\bullet+}$, as electron carrier. The reduced relay is generated through a photochemical system that includes deazariboflavin, dRFl (**1**), as photosensitizer, *N,N'*-dimethyl-4,4'-bipyridinium, MV^{2+}, as electron acceptor, and oxalate as sacrificial electron donor.

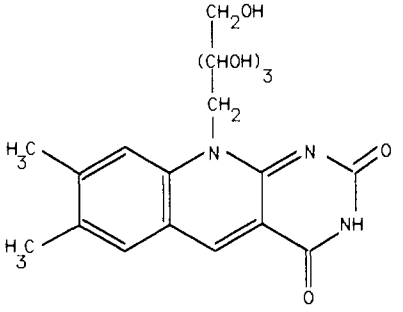

(1)

Experimental Section

Absorption spectra were recorded with an Uvikon-860 (Kontron) spectrophotometer equipped with a thermostated cell holder that includes a magnetic stirring motor at the bottom of the unit. NMR spectra were recorded on a 200-MHz instrument (Brucker). A Philips 300 M transmission electronmicroscope was used to determine the size of colloid particles. X-ray diffraction analyses were performed on a Philips powder diffractometer. Continuous illumination experiments were performed with a 1000-W halogen-quartz lamp, and light was filtered through a 400-nm filter. Incident photon flux was determined by Reinecke salt actinometry[32] to be 1×10^{-3} einstein·M^{-1}·min^{-1}. Laser flash experiments were carried out with a dye laser (DL-12 Molectron) pumped by a nitrogen laser (UV-14 Molectron).

Palladium content in the various colloids was determined by atomic absorption (Perkin-Elmer 403 apparatus). Formate was analyzed by ion chromatography using a Wescan anion-exclusion column, 2×10^{-3} N H_2SO_4 was eluent, and detection was performed with a conductivity detector (Knauer). Hydrogen was analyzed by gas chromatography (Hewlett-Packard 5890 Instrument) with a 5-Å molecular sieve column and argon as carrier gas. The production of $MV^{\bullet+}$ was followed spectroscopically at 602 nm ($\epsilon = 1.3 \times 10^4$ M^{-1}·cm^{-1}).[33]

Chemicals were obtained from Aldrich. Deazariboflavin (**1**) was prepared according to the literature.[34] DCO_2Na was prepared by hydrolysis of NaCN in D_2O, and the product was recrystallized from ethanol-water.[35] A solution of sodium hydrogen [^{13}C]carbonate was prepared by bubbling $^{13}CO_2$ through a 0.1 M NaOH solution until pH = 7.0.

The active Pd-β-CD colloid for CO_2/HCO_3^- photoreduction is prepared by heating while stirring, a 1.5×10^{-3} M Na_2PdCl_4 solution that includes β-cyclodextrin (1% w/w) at 60 °C for $2^1/_2$ h. The color of the solution changes from yellow to dark brown. The resulting colloid is deionized with small amounts of Amberlite MB-1 to exclude remains of $PdCl_4^{2-}$ (purification of the colloid from $PdCl_4^{2-}$ is followed spectroscopically). The resulting colloid is centrifuged (3500 rpm for 10 min) to exclude any precipitated palladium. It should be noted that a decrease in the Pd-β-CD catalyst activity has been observed upon aging. Also, in a series of 10 different batches of the Pd-β-CD colloid we observe up to a 5-fold difference between the most active and least active colloids. The inactive Pd-β-CD catalyst is prepared by a similar procedure, but the temperature of the reaction mixture is maintained at 90 °C. The Pd colloid stabilized by D-glucose was prepared by a method similar to that for Pd-β-CD except that the D-glucose content in the aqueous solution is 0.67% (w/w). Pd colloid stabilized by polyvinylpyrrolidinone is prepared by either H_2 bubbling or $NaBH_4$ addition to an aqueous 1.5×10^{-3} M Na_2PdCl_4 solution that contains polyvinylpyrrolidone (1% w/w).

Samples of Pd-β-CD for electron microscopy were prepared by the following procedure: A copper colloidon-coated grid was placed on a small cork and the cork mounted in a centrifuge test tube. The tube was filled with a 1:1 mixture of Pd-β-CD colloid and 1% gelatin solution and vertically centrifuged (8000 rpm for 20 min). The solution was decanted and the grid was washed with triply distilled water and dried. Samples for X-ray diffraction were prepared by a similar method: A glass plate was mounted on the cork support, and Pd was deposited on the glass plate by centrifugation. The glass plate with deposited Pd was analyzed after drying.

The systems for continuous illumination experiments consisted of a 0.1 M $NaHCO_3$ aqueous solution that included sodium oxalate (5×10^{-2} M) as electron donor, deazariboflavin (3×10^{-5} M) as photosensitizer, *N,N'*-dimethyl-4,4'-bipyridinium, (methyl viologen, MV^{2+}; 1×10^{-3} M) as electron acceptor, and Pd-β-CD (40 mg·L^{-1}) as catalyst. The solution (3 mL) was placed in a glass cuvette, equipped with a microstirrer and serum stopper. The solution in the cuvette was flushed with oxygen-free carbon dioxide and illuminated, $\lambda > 400$ nm (resulting pH = 6.8-7.0). Aliquots were taken out at time intervals of illumination and analyzed for HCO_2^-. The gaseous atmosphere was analyzed for H_2. The kinetics studies of HCO_2^- photogeneration as a function of HCO_3^- concentration were performed in an aqueous system, 3 mL, that consisted of phosphate buffer (7×10^{-2} M), sodium oxalate (5.5×10^{-2} M), deazariboflavin (3×10^{-5} M), MV^{2+} (1×10^{-3} M), and Pd-β-CD (40 mg·L^{-1}). The system was flushed with argon, and varying amounts of an aqueous 4.3×10^{-1} M $NaHCO_3$ stock solution were injected into the system, which was equilibrated for 10 min before illumination. The kinetics of MV^{2+} reduction by HCO_2^- were followed in the following way: 2.9 mL of an aqueous phase that included MV^{2+} (1×10^{-3} M) and Pd-β-CD (45

(21) (a) Wiener, H.; Sasson, Y. *J. Mol. Catal.* **1986**, *35*, 277. (b) Kuda, K.; Sugita, N.; Takezaki, Y. *Nippon Kagaku Kaishi* **1977**, 302.
(22) Stalder, C. J.; Chao, S.; Summers, D. P.; Wrighton, M. S. *J. Am. Chem. Soc.* **1983**, *105*, 6318.
(23) (a) Stalder, C. J.; Chao, S.; Wrighton, M. S. *J. Am. Chem. Soc.* **1984**, *106*, 3673. (b) Chao, S.; Stalder, C. J.; Summers, D. P.; Wrighton, M. S. *J. Am. Chem. Soc.* **1984**, *106*, 2723.
(24) (a) Lehn, J.-M.; Ziessel, R. *Proc. Natl. Acad. Sci. U.S.A.* **1982**, *79*, 701. (b) Hawecker, J.; Lehn, J.-M.; Ziessel, R. *J. Chem. Soc., Chem. Commun.* **1983**, 536.
(25) Hawecker, J.; Lehn, J.-M.; Ziessel, R. *J. Chem. Soc., Chem. Commun.* **1985**, 56.
(26) (a) Maidan, R.; Willner, I. *J. Am. Chem. Soc.* **1986**, *108*, 8100. (b) Willner, I.; Maidan, R.; Mandler, D.; Dürr, H.; Dörr, G.; Zengerle, K. *J. Am. Chem. Soc.* **1987**, *109*, 6080.
(27) (a) Aurian-Blanjeni, B.; Halmann, M.; Manassen, *J. Sol. Energy* **1980**, *25*, 165. (b) Inoue, T.; Fujishima, A.; Konishi, S.; Honda, K. *Nature* **1979**, *277*, 637.
(28) (a) Bradley, M. G.; Tysak, T.; Gravea, D. J.; Vlachopoulos, N. A. *J. Chem. Soc., Chem. Commun.* **1983**, 349. (b) Halmann, M. *Nature* **1978**, *275*, 115.
(29) (a) Parkinson, B. A.; Weaver, P. F. *Nature* **1984**, 148. (b) Mandler, D.; Willner, I. *J. Chem. Soc., Perkin Trans. 2*, in press.
(30) (a) Ziessel, R.; Hawecker, J.; Lehn, J.-M. *Helv. Chim. Acta* **1986**, *69*, 1065. (b) Hawecker, J.; Lehn, J.-M.; Ziessel, R. *Ibid.* **1986**, *69*, 1990.
(31) (a) Ishida, H.; Tanaka, K.; Tanaka, T. *Chem. Lett.* **1987**, 1035. (b) Kitamura, N.; Tazuke, S. *Chem. Lett.* **1983**, 1109.
(32) Wegner, E. E.; Adamson, A. W. *J. Am. Chem. Soc.* **1966**, *88*, 394.
(33) Thorneley, R. N. F. *Biochim. Biophys. Acta* **1974**, *333*, 487.
(34) Ashto, T. W.; Brown, R. D.; Tolman, R. L. *J. Heterocycl. Chem.* **1978**, *15*, 489.
(35) Rapp, G. A.; Melton, C. E. *J. Am. Chem. Soc.* **1958**, *80*, 3509.

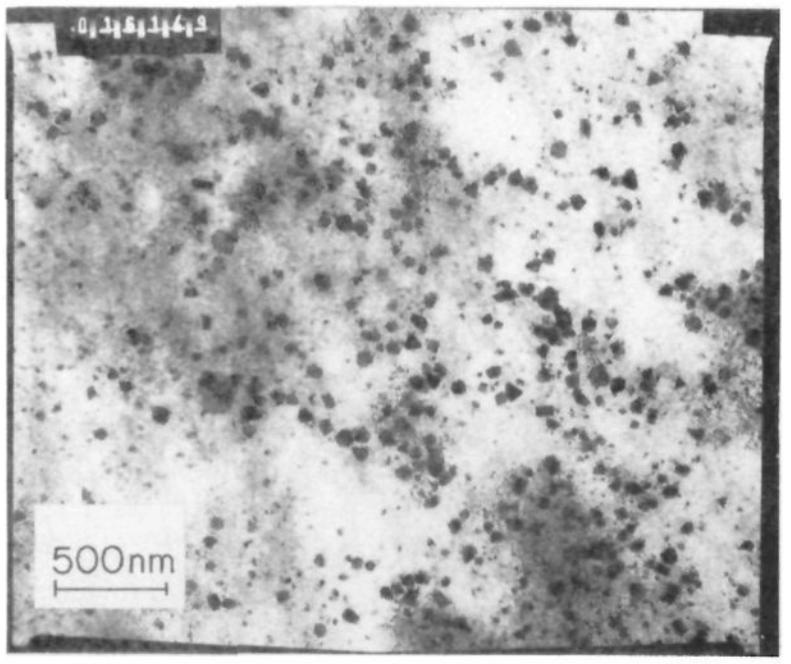

Figure 1. Transmission electron micrograph of active Pd–β-CD colloid.

mg·L^{-1}) was deaerated with argon and thermostated to the desired temperature. To the resulting solution, mounted in the spectrophotometer, 0.1 mL of sodium formate stock solution was injected (final concentration 1×10^{-1} M). The $MV^{\bullet+}$ formation was followed at $\lambda = 602$ nm. In order to avoid varying activities of the Pd–β-CD in D_2O as a result of the preparation procedures, this colloid was not prepared by direct reduction of $PdCl_4^{2-}$ in D_2O but through an alternative route: The Pd–β-CD colloid in H_2O was lyophilized to dryness, and the resulting Pd–β-CD powder was resuspended in D_2O by vortex stirring. Control experiments revealed that the activity of Pd–β-CD colloid was unaffected by the lyophilization/resuspension processes.

Properties of Pd Colloids as Catalysts for HCO_3^- Photoreduction

We find that Pd colloids can be stabilized by cyclodextrins similarly to other metals, i.e.., Rh or Pt. We also prepared Pd colloids stabilized by other stabilizing supports such as glucose and polyvinylpyrrolidone. In the present study we mainly characterize the catalytic activities of Pd colloids stabilized by β-cyclodextrins, Pd–β-CD, in the reduction of HCO_3^- to formate and in the reverse process. Some of the catalytic properties of the Pd colloids stabilized by the other supports are also provided. We find that the procedure whereby the Pd–β-CD colloid is prepared, dramatically affects its catalytic activity. Preparation of the Pd colloid at 60 °C results in an active catalyst for bicarbonate reduction to formate. In the absence of bicarbonate this catalyst is active in H_2 evolution. This catalyst is also catalytically active in the reverse process that oxidizes formate to bicarbonate. In turn, Pd–β-CD colloid prepared at 90 °C is inactive toward HCO_3^- reduction or the reverse oxidation of formate, but is catalytically active in H_2 evolution. The Pd–β-CD colloid is stable for prolonged periods of time, namely, for at least a month. Hydrogen effects aggregation of the colloid, presumably due to interparticle H_2 adsorption. These colloids can be dried through lyophilization. The resulting brown powders can be resuspended in aqueous solution. The regenerated colloids exhibit similar catalytic activities as compared to the original Pd–β-CD colloids. This property of the Pd–β-CD colloid allows the long-term storage of the catalyst. In the present study we prepared Pd–β-CD colloids in D_2O (vide infra) by resuspension of the Pd–β-CD powder in D_2O.

The electron micrograph of the active Pd–β-CD colloid is shown in Figure 1. The metal particles exhibit a broad size distribution in the range of 200–1200 Å. The X-ray diffraction patterns of either the active or inactive Pd–β-CD colloids show diffraction bands at angles $2\theta = 40.0$, 46.5, and 67.9°. These diffraction angles are characteristic of crystalline Pd metal in cubic crystal structure.

Similarly, Pd colloids that are active toward the reduction of HCO_3^- and oxidation of formate were prepared by using α-cyclodextrin, glucose, or polyvinylpyrrolidone as stabilizing supports. With the polyvinylpyrrolidone support, $NaBH_4$ or hydrogen were used as reducing agents of $PdCl_4^{2-}$. Only the Pd colloids stabilized by cyclodextrins could be lyophilized to powdered catalysts that can be resuspended into aqueous stable colloids.

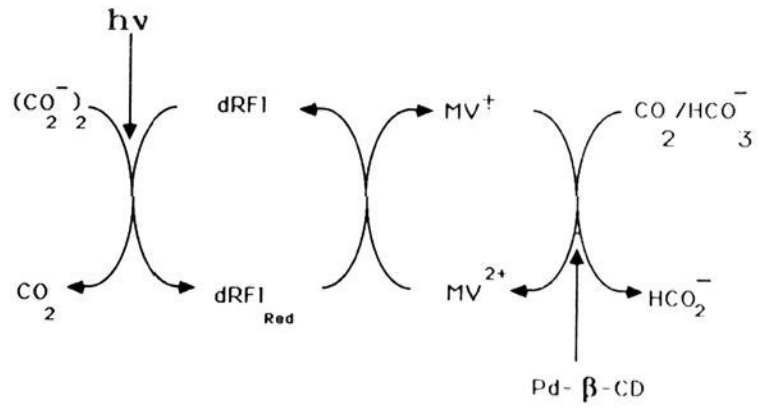

Figure 2. Schematic cycle for the photosensitized reduction of HCO_3^- to formate.

Photoreduction of CO_2/HCO_3^- to Formate

We have examined the catalyzed reduction of CO_2/HCO_3^- using the Pd–β-CD colloid and photogenerated *N*,*N*′-dimethyl-4,4′-bipyridinium radical cation, $MV^{\bullet+}$, as electron carrier for the process. The photosystem for the generation of $MV^{\bullet+}$ is composed of deazariboflavin, dRFl (**1**), as photosensitizer, *N*,*N*′-dimethyl-4,4′-bipyridinium, methyl viologen, MV^{2+}, as electron acceptor, and oxalate as sacrificial electron donor (Figure 2). The reduction of MV^{2+} in this specific system has been examined previously by Krasna[36] and proceeds with a quantum efficiency of $\phi = 3.6$. The high quantum yield obtained with **1** as photosensitizer is due to complex redox properties of reduced flavin dyes[37] and to several reduction equivalents formed upon oxidative decomposition of the sacrificial electron donor. It should be noted that this unusual photosystem is selected for the production of $MV^{\bullet+}$ for two reasons: (i) Common sacrificial electron donors act as inhibitors for the catalyst (vide infra) and eliminate kinetic characterization. (ii) To characterize the kinetic activity of the Pd–β-CD colloid, the overall rate of CO_2/HCO_3^- reduction should not be controlled by the rate of generation of the primary electron carrier, $MV^{\bullet+}$. The effectiveness of $MV^{\bullet+}$ photogeneration with this photosystem provides a means that meets this requirement.

Illumination of an aqueous bicarbonate solution, pH = 6.8, that includes dRFl as sensitizer, MV^{2+} as primary charge relay, and oxalate as electron donor results in the formation of methyl viologen radical $MV^{\bullet+}$. In the presence of either of the two Pd–β-CD colloids, the reduced methyl viologen mediates different reduction processes: In the prescence of the Pd–β-CD colloid prepared at 60 °C reduction of CO_2/HCO_3^- to formate occurs (Figure 3), and only trace amounts of H_2 are generated. In turn, in the presence of the Pd–β-CD colloid prepared at 90 °C only

(36) Krasna, A. I. *Photochem. Photobiol.* **1980**, *31*, 75.

(37) A chain mechanism outlined in the following set of reactions presumably leads to the high quantum efficiency of $MV^{\bullet+}$ (D = dRFl), Cf.: Bliese, M.; Launikonis, A.; Loder, J. W.; Mau, A. W.-H.; Sasse, W. H. F. *Aus. J. Chem.* **1983**, *36*, 1873.

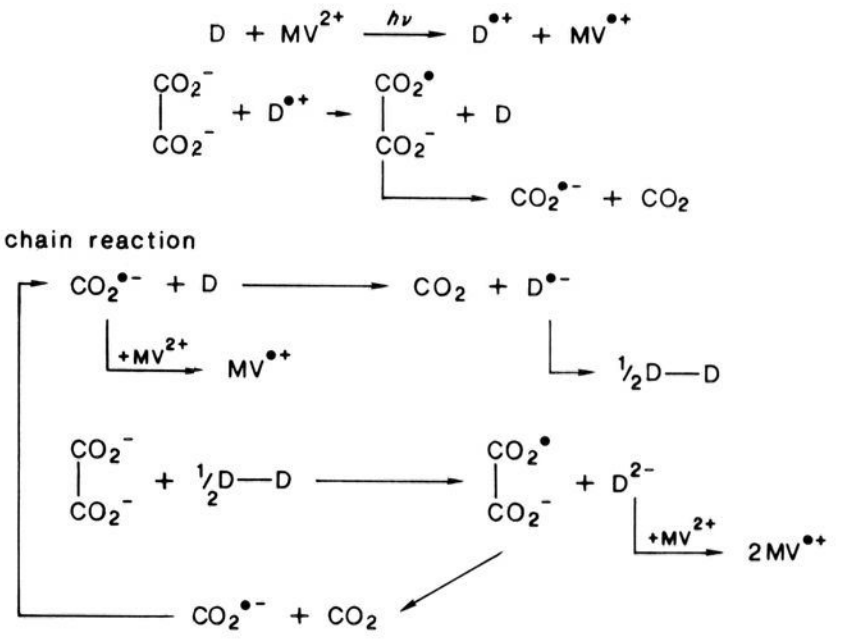

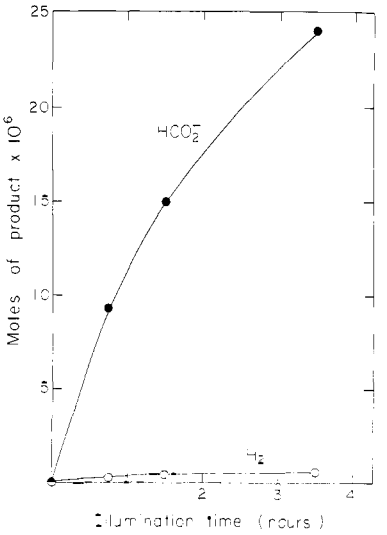

Figure 3. Rates of HCO_2^- and H_2 formation at the intervals of illumination using the active Pd-β-CD catalyst.

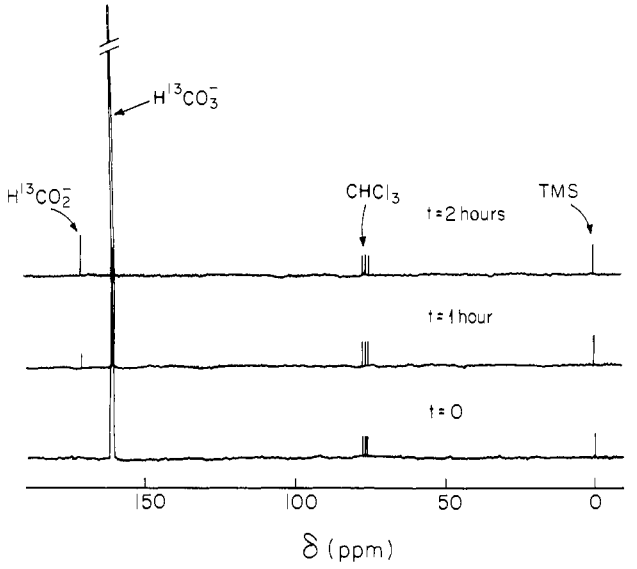

Figure 4. ^{13}C NMR spectra of samples taken at time intervals of illumination of the photochemical assembly using $H^{13}CO_3^-$ as substrate.

photoinduced H_2 evolution proceeds and no formate could be detected. Figure 3 shows the rates of formate generation and H_2 evolution as a function of illumination time using the active HCO_3^- reduction colloid. The quantum yield for formate formation corresponds to $\phi = 1.1$. It should be noted that illumination of the system in the absence of CO_2/HCO_3^- and in the presence of the active Pd-β-CD bicarbonate reduction colloid results in effective H_2 evolution, $\phi = 0.12$, and no formate is detected. These results clearly indicate that the Pd-β-CD colloid prepared at 60 °C acts as a hydrogen catalyst as well as a CO_2/HCO_3^- reduction catalyst. Nevertheless, the latter process is favored in the presence of the substrate CO_2/HCO_3^-.

The lack of formate formation in the absence of the substrate indicates that HCO_2^- originates from CO_2/HCO_3^- rather than from an oxidative decomposition route of the oxalate electron donor. This has been firmly confirmed by using [^{13}C]bicarbonate as substrate in the photochemical system. Figure 4 shows the ^{13}C NMR spectra of the system at time intervals of illumination. It is evident that $H^{13}CO_2^-$, $\delta = 171.2$ ppm, is gradually formed as illumination proceeds.

Pd-β-CD Catalyzed Reduction of Bicarbonate

Kinetics of Bicarbonate Reduction. The Pd-catalyzed reduction of bicarbonate by hydrogen to form formate has been reported to proceed through hydrogenation of HCO_3^- by Pd-bound hydrides. These are formed upon dissociation of H_2 on the metal catalyst. Similarly, the photosensitized H_2-evolution process using *N,N'*-dimethyl-4,4'-bipyridinium, MV^{2+}, as charge relay and various metal colloids as catalysts has been extensively studied.[38] It has been shown that metal-bound hydrogen atoms (or hydrides) are formed through a sequential mechanism that involves the charging of the metal colloid by the photoreduced relay $MV^{\bullet+}$, followed by protonation of the charged metal (eq 8, 9). These

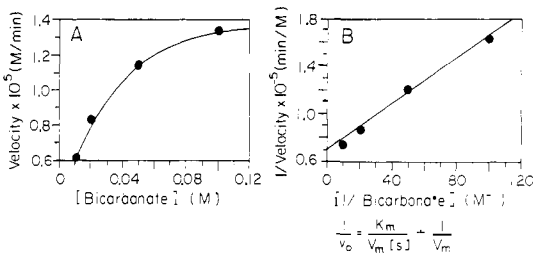

Figure 5. (A) Initial rates of HCO_2^--photoinduced formation as a function of substrate (HCO_3^-) concentration. (B) Graphic representation of the reciprocals of the initial rates as a function of the reciprocals of the substrate concentration ($1/HCO_3^-$). In all experiments [dRFl] = 3×10^{-5} M, $[MV^{2+}] = 1 \times 10^{-3}$ M, $[(CO_2Na)_2] = 5.5 \times 10^{-2}$ M, and Pd-β-CD = 40 mg·L^{-1}.

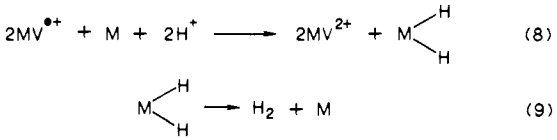

observations allow us to suggest the sequence of reactions outlined in eq 10–13 as the mechanistic steps involved in the photoreduction

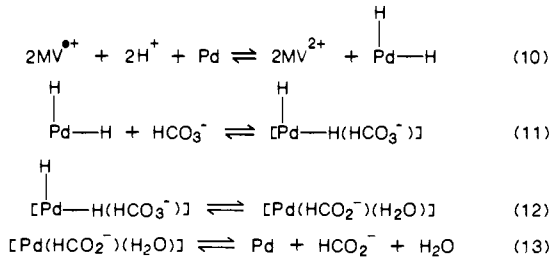

of HCO_3^- to formate. In the primary step, photogenerated $MV^{\bullet+}$ generates Pd-bound hydrides (eq 10). The Pd catalyst also activates HCO_3^- through the formation of an activated complex structure, wherein hydrogenation of bicarbonate to formate occurs by discharge of the Pd hydrides.

We have examined the rates of photoinduced formate production as a function of the bicarbonate substrate concentration, and at a constant Pd content of 45 mg·L^{-1}. Figure 5A shows the initial rates of HCO_2^- generation at different bicarbonate concentrations under continuous illumination. It is evident that the rate increases as the substrate concentration is increased and the rate levels off at an approximate substrate concentration of $[HCO_3^-] = 0.1$ M. Such behavior could originate if specific sites for bicarbonate activation and reduction are present on the Pd-β-CD catalyst. Namely, the leveling off in the rates of HCO_2^- formation originates from saturation of these active sites by the HCO_3^-. In the sequence of reactions that leads to formate, the photogeneration of $MV^{\bullet+}$ proceeds with a quantum yield of $\phi = 3.6$. The fact that the quantum yield of formate generation ($\phi = 1.1$) is lower than that of $MV^{\bullet+}$ production suggests that the rate of formate production is limited by a dark catalytic process rather than by the photochemical reaction. Indeed, under steady-state illumination $MV^{\bullet+}$ is accumulated in the system. It is also well documented[39] that the interaction of a reduced relay

(38) (a) Grätzel, M., Ed. *Energy Resources through Photochemistry and Catalysis*; Academic Press: New York, 1983; and references therein. (b) Harriman, A., West, M. A., Eds. *Photogeneration of Hydrogenation*; *Academic* Press: London, 1983.

with the metal catalyst to form metal-bound hydrides is a rapid process. Thus, it is conceivable that the formation of the activated complex (eq 11) and subsequent reduction of bicarbonate (eq 12) are rate limiting in HCO_2^- photogeneration. This analysis suggests that the activity of Pd–β-CD colloid in the photosensitized reduction of bicarbonate is analogous to the active site–substrate model in enzyme activities. Hence the kinetic activity of the Pd–β-CD colloid should follow well-established enzyme kinetics relationship.[40]

Consequently, the relation of the initial rates of formate generation as a function of bicarbonate concentration is given by eq 14. Indeed, analysis of the saturation curve (eq 15) through

$$v_0 = \frac{V_{max}[HCO_3^-]}{K_m + [HCO_3^-]} \quad (14)$$

$$\frac{1}{v_0} = \frac{1}{V_{max}} + \frac{K_m}{V_{max}} \frac{1}{[HCO_3^-]} \quad (15)$$

plotting $1/v_0$ vs $1/[HCO_3^-]$ results in a linear relationship (Figure 5B). The derived values of K_m and V_{max} are $K_m = (1.5 \pm 0.6) \times 10^{-2}$ M and $V_{max} = (1.5 \pm 0.3) \times 10^{-5}$ M/min.

A second aspect that has been considered in the activities of the Pd–β-CD colloids relates to kinetic isotopes effects involved in CO_2/HCO_3^- photoreduction and H_2-evolution processes, using the various colloids. The rate of CO_2/DCO_3^- photoreduction in D_2O is not affected as compared to that in H_2O. In turn, a significant isotope effect is observed in the hydrogen-evolution process, $K_H/K_D \approx 3$. The observation of an isotope effect in the H_2-evolution process using the Pd catalyst is consistent with previous studies that explored the photosensitized H_2 evolution through interaction of generated radicals with Pt and Au colloids.[41] These studies revealed that charging the metal by the reduced relay and formation of surface-bound hydrogen atoms are rapid reactions, while the discharge of hydrogen atoms through cleavage of metal–hydrogen bonds is rate limiting in H_2 evolution. Thus, our results imply that the rate-limiting step in H_2 evolution in the presence of the Pd–β-CD catalyst involves the cleavage of a Pd–H bond (eq 16), but the rate of HCO_2^- formation is not controlled by cleavage of these bonds.

$$\text{Pd—H} + H_2 \longrightarrow \text{Pd} \quad (16)$$

Inhibition Effects in the Reduction of Bicarbonate. The catalytically active Pd–β-CD colloid for bicarbonate reduction exhibits high sensitivity toward various additives. We find that aldehydes, amines, and particularly thiols act as inhibitors for the catalyst toward bicarbonate reduction. We have studied in detail the effect of added mercaptoethanol, $HOCH_2CH_2SH$, on the kinetics of the photosensitized formate formation. Figure 6A shows the rate of formate formation at different mercaptoethanol concentrations. It is evident that as the concentration of the thiol is increased, the rate of formate formation declines, and at an inhibitor concentration of $[HOCH_2CH_2SH] = 2 \times 10^{-4}$ M, the photoinduced formation of HCO_2^- is completely blocked. Simultaneous to the inhibition in formate generation with added mercaptoethanol, H_2 evolution from the system occurs. Figure 6C shows the rate of H_2 evolution upon illumination of the system at different thiol concentrations. We realize that the rate of photosensitized H_2 evolution increases as the concentration of mercaptoethanol is increased. At a thiol concentration of $[HOCH_2CH_2SH] = 2 \times 10^{-4}$ M, where formate formation is entirely blocked, the rate of H_2 evolution is similar to that observed from the system in the absence of the bicarbonate. Thus, in the presence of mercaptoethanol, formate generation is inhibited and the catalyst activity

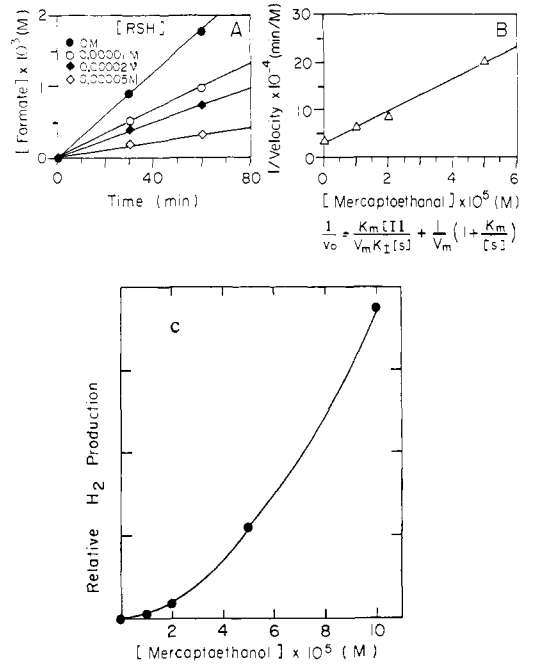

Figure 6. (A) Rates of photoinduced HCO_2^- formation of different concentrations of the inhibitor mercaptoethanol. (B) Graphic representation of the reciprocals of rates as a function of inhibitor concentration. (C) Relative rates of H_2 evolution at different concentrations of mercaptoethanol. In all experiments [dRFl] = 3×10^{-5} M, [MV2+] = 1×10^{-3} M, $[(CO_2Na)_2] = 5.5 \times 10^{-2}$ M, $[HCO_3^-] = 0.1$ M, and Pd–β-CD = 40 mg·L^{-1}.

toward H_2 evolution (present in the absence of CO_2/HCO_3^-) is restored. Our results reveal that the active Pd–β-CD catalyst toward HCO_3^- reduction includes two characteristic types of active sites. One class of sites is catalytically active in the generation of surface-bound H-atoms, sites that subsequently effect H_2 evolution. The second type of sites is responsible for bicarbonate activation. In the absence of inhibitor, hydrogenation of activated HCO_3^- by surface-bound hydrides proceeds, rather than H_2 evolution, since the former process is faster. Added mercaptoethanol blocks selectively the bicarbonate activation sites, and consequently, only the rather slow H_2 evolution process occurs.

The inhibition phenomenon observed in the presence of added thiol suggests that the activation of bicarbonate on its active sites (eq 11) is competitively inhibited by binding of mercaptoethanol to the same sites (eq 17). Therefore, the kinetics of the bi-

$$\text{Pd—H} + RSH \rightleftharpoons \text{Pd—H(RSH)} \quad (17)$$

carbonate reduction process with added mercaptoethanol should follow the rate equations for competitive inhibition of an active site–substrate activated complex. Under such conditions, the relation between the initial rate of formate formation as a function of the inhibitor concentration should be given by eq 18, where K_I is the dissociation constant of the inhibitor–catalyst complex.

$$v_0 = \frac{V_{max}}{1 + \frac{K_m}{[HCO_3^-]}\left(1 + \frac{[HOCH_2CH_2SH]}{K_I}\right)} \quad (18)$$

$$K_I = \frac{[\text{H-Pd-H}][HOCH_2CH_2SH]}{[\text{H-Pd-H}(HOCH_2CH_2SH)]}$$

$$\frac{1}{v_0} = \frac{K_m[HOCH_2CH_2SH]}{V_{max}K_I[HCO_3^-]} + \frac{1}{V_{max}}\left(1 + \frac{K_m}{[HCO_3^-]}\right) \quad (19)$$

Figure 6B shows that a linear correlation is obtained upon plotting $1/v_0$ (where v_0 is the initial rate of HCO_2^- formation) as a function of mercaptoethanol concentration (eq 19) at a

(39) (a) Meisel, D.; Mulac, M.; Matheson, D. *J. Phys. Chem.* **1981**, *85*, 179. (b) Meisel, D. *J. Am. Chem. Soc.* **1979**, *101*, 6133. (c) Henglein, A. *Angew. Chem.* **1979**, *91*, 449. (d) Henglein, A.; Lilie, J. *J. Am. Chem. Soc.* **1981**, *103*, 1059.

(40) Segel, I. H., Ed.; *Enzyme Kinetics*; Wiley: New York, 1975.

(41) Kopple, K.; Meyerstein, D.; Meisel, D. *J. Phys. Chem.* **1980**, *84*, 870, and references therein.

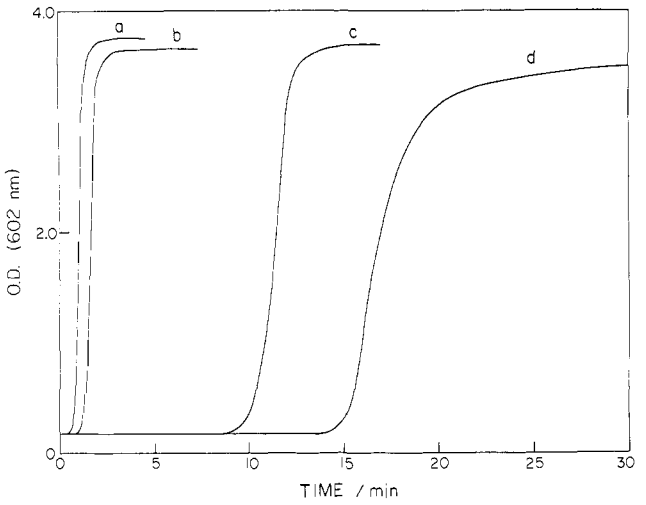

Figure 7. Rate profiles for the dark reduction of MV^{2+} by HCO_2^- at different temperatures followed spectroscopically at λ = 602 nm; (a) 37 °C, (b) 30 °C, (c) 20 °C, (d) 10 °C. In all experiments $[MV^{2+}] = 1 \times 10^{-3}$ M, $[HCO_2^-] = 0.1$ M, Pd-β-CD = 45 mg·L^{-1}.

constant concentration of HCO_3^-. This implies that the bicarbonate activation sites are indeed blocked by the thiol through a competitive inhibition mechanism. From this plot the value $K_I = (2.9 \pm 1.5) \times 10^{-6}$ M^{-1} is derived.

Pd-β-CD Catalyzed Oxidation of Formate

Kinetics of Formate Oxidation. Similar to enzymes that often exhibit reversible activities, the Pd-β-CD colloids show similar reversible properties. The Pd-β-CD colloid that is active in the photoreduction of HCO_3^- to formate shows reversible activity, and formate reduces MV^{2+} to $MV^{\bullet+}$ in the presence of the catalyst (eq 20). In turn, the inactive Pd-β-CD catalyst (prepared at 90 °C) does not exhibit catalytic activity toward this process. Figure 7 shows the rate of MV^{2+} reduction to $MV^{\bullet+}$ by formate in the presence of the active Pd-β-CD colloid at various temperatures. It can be seen that the formation of $MV^{\bullet+}$ is triggered after an induction period. Thereafter, $MV^{\bullet+}$ accumulates and levels off to establish a steady-state concentration. As the temperature of the system increases, the induction period for $MV^{\bullet+}$ formation is shortened, the accumulation of $MV^{\bullet+}$ is enhanced, and a similar steady-state concentration of $MV^{\bullet+}$ is formed at the different temperatures. It should be noted that at the time scales of these experiments only trace amounts of H_2 are formed. The reduction of MV^{2+} by formate is expected to proceed through the reverse reactions (eq 21–23) that were previously detailed for bicarbonate

$$HCO_2^- + Pd + H_2O \rightleftharpoons Pd(H_2O)(HCO_2^-) \quad (21)$$

$$Pd(H_2O)(HCO_2^-) \rightleftharpoons Pd(H)(HCO_3^-) \quad (22)$$

$$Pd(H) + 2MV^{2+} \rightleftharpoons 2MV^{\bullet+} + Pd + 2H^+ \quad (23)$$

reduction to formate, i.e., activation of formate followed by its oxidation to HCO_3^- and Pd hydride formation, and subsequent reduction of MV^{2+} by the Pd hydride. Since the evolution of hydrogen (eq 16) is slow, this process can be disregarded and $MV^{\bullet+}$ is formed through the sequential processes, eq 21–23. The induction time required for the generation of $MV^{\bullet+}$ is attributed to the buildup of Pd hydrides that is the rate-limiting process. Once the threshold concentration of hydrides is formed, the reduction of MV^{2+} is triggered. Subsequently, the rate of $MV^{\bullet+}$ accumulation (slope) corresponds to the rate of Pd hydrides formation in the system, which is the rate-limiting process. It is also evident from Figure 7 that as the temperature is increased, the induction period is shortened and the rate of $MV^{\bullet+}$ formation (slope) is enhanced, implying that the formation of Pd hydrides

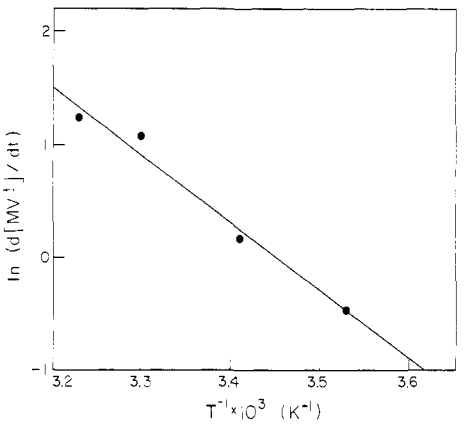

Figure 8. Arrhenius plot for the dark reduction of MV^{2+} by HCO_2^-.

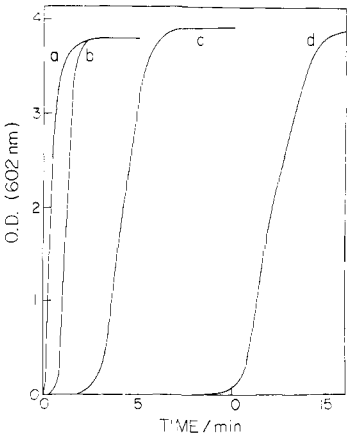

Figure 9. Rate profiles for the dark reduction of MV^{2+} by formate in water: (a) by HCO_2^- in H_2O; (b) by HCO_2^- in D_2O; (c) by DCO_2^- in H_2O; (d) by DCO_2^- in D_2O. In all experiments $[MV^{2+}] = 1 \times 10^{-3}$ M; [formate] = 0.1 M; 28 °C.

is increased as the temperature rises. From these curves the observed rate constants, k_{obsd}, were calculated at various temperatures. The Arrhenius plot (Figure 8) of the observed rate constants for the reduction of MV^{2+} by formate gives an activation barrier of $E_a = 13$ kcal·mol^{-1} for the process. Since the thermodynamic balance for the process outlined in eq 20 is close to $\Delta G \approx 0$ kcal·mol^{-1}, we deduce that the activation barrier for the reduction of bicarbonate to HCO_2^- exhibits a similar value.

Reduction of MV^{2+} by formate is also inhibited by added mercaptoethanol, $HOCH_2CH_2SH$. As the inhibitor concentration increases, the induction period is longer and the rate of $MV^{\bullet+}$ formation is retarded. These results suggest that formate is activated toward production of Pd hydrides on the similar sites that lead to activation of bicarbonate and its hydrogenation to formate. Mercaptoethanol acts as a competitive inhibitor to HCO_2^- for these active sites.

Isotope Effects in Formate Oxidation. A second aspect that has been considered in the kinetics of MV^{2+} reduction by formate involved the determination of kinetic isotope effects in the reaction. Figure 9 compares the rate of reduction of MV^{2+} by HCO_2^- in H_2O to the rates of MV^{2+} reduction by DCO_2^- in H_2O, by HCO_2^- in D_2O, and by DCO_2^- in D_2O. We realize that using DCO_2^- in H_2O or D_2O results in an isotope effect of $k_H(HCO_2^-)/k_D(DCO_2^-) = 4.8 \pm 1.1$ in H_2O and of $k_H(HCO_2^-)/k_D(DCO_2^-) = 4.2 \pm 0.7$ in D_2O. Isotope effects are also observed with D_2O instead of H_2O; $k_H(H_2O)/k_D(D_2O) = 1.5 \pm 0.3$ and $k_H(H_2O)/k_D(D_2O) = 1.3 \pm 0.2$ in HCO_2^- and DCO_2^-, respectively. When the composition of DCO_2^- in D_2O is used, the multiple of the two isotope effects, $k_H/k_D = 6.34 \pm 1.2$ is observed ($k_H/k_D = 6.4$ calculated). Thus, we conclude that the rate-limiting step in the reduction process of MV^{2+} by formate involves the cleavage of C–H in formate and H–OH in water. This conclusion is consistent with other reports[21] in which the kinetic isotope effects

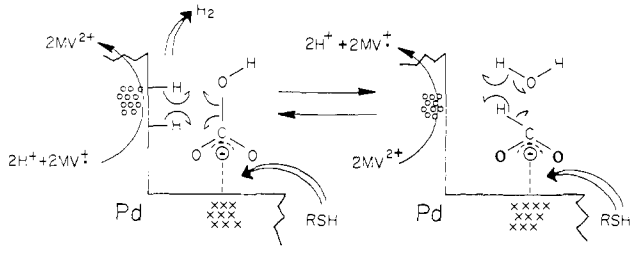

Figure 10. Schematic sequential mechanism for the Pd–β-CD catalyzed reduction of HCO_3^- to formate and the reverse process.

in the decomposition of formate to hydrogen over a Pd/C catalyst were examined, where cleavage of H-bonds in formate and water participate in the rate-limiting process.

Mechanistic Aspects Involved in the Photoreduction of CO_2/HCO_3^- to Formate. The possible participation of the stabilizing support of the Pd colloid, β-cyclodextrin, in the activation of the bicarbonate substrate toward reduction to HCO_2^- has been examined. Cyclodextrins are cyclic macromolecular structures of glucose that form cylindrical cavities capable of associating various substrates. We have performed several experiments that exclude the operative participation of the β-CD receptor in the activation of HCO_3^-: (i) Addition of *N*-octylpyridinium bromide to the photochemical system that leads to the reduction of HCO_3^- to formate does not affect the rate of HCO_2^- production. Since *N*-octylpyridinium binds to the β-CD cavity, any activation of HCO_3^- through the β-CD cavity should be inhibited. (ii) We find that various other Pd colloids that are stabilized by supports that lack a cavity structure are also active in the photoreduction of HCO_3^- to formate. For example, Pd stabilized by glucose or polyvinylpyrrolidone exhibits catalytic activity toward CO_2/HCO_3^- photoreduction to formate. In this context, it is worthwhile to state that a rapid test of Pd colloid activities toward reduction of HCO_3^- to formate can be performed by examination of the reverse process, i.e., reduction of MV^{2+} by formate. We find that all colloids that were catalytically active in the reverse process were also active in the photoreduction of HCO_3^- to formate.

We have examined in the present study various aspects related to the catalytic activity of the Pd–β-CD colloid toward the photoreduction of bicarbonate to formate and the reverse oxidation of HCO_2^-. The different mechanistic details provide, when united, a comprehensive model that accounts for the catalytic properties of Pd–β-CD in these processes. The Pd–β-CD catalyst includes two types of active sites (Figure 10): One type generates Pd hydrides, while the other catalytic sites activate bicarbonate toward reduction. The primary step in the photoreduction of HCO_3^- involves charging of the metal particles and formation of Pd hydrides (eq 10). Since the H_2 evolution process is slow, hydrogenation of activated bicarbonate proceeds effectively (eq 12). In the presence of the inhibitor mercaptoethanol, selective inhibition of the bicarbonate activation sites occurs. Consequently, the slow H_2-evolution process predominates as the only route that utilizes the Pd–H intermediates. The reverse process where formate reduces MV^{2+}, involves the similar Pd–H intermediate. The rate-limiting step for $MV^{\bullet+}$ production involves the formation of the Pd–H intermediate, as evidenced by the induction period observed in the kinetic profile of $MV^{\bullet+}$ formation. We revealed that the rate-limiting step in the reverse reaction involves the cleavage of C–H and H–OH bonds of formate and water, respectively. These results suggest that formation of the Pd–H intermediate proceeds through a concerted mechanism that is displayed in Figure 10. Inhibition of the reverse process by thiols implies that activation of formate toward oxidation occurs on the similar sites that activate HCO_3^- for hydrogenation.

Conclusions

We have highlighted that a Pd–β-CD colloid acts as an artificial heterogeneous catalyst for CO_2/HCO_3^- reduction to formate that mimics enzyme activities: (i) It exhibits high specificity and effectiveness toward CO_2/HCO_3^- reduction; (ii) it is competitively inhibited toward the substrate activation and reduction; (iii) it reveals "enzyme-like" kinetics; and (iv) it shows reversible properties. Previously,[29] we have shown that the enzyme formate dehydrogenase acts as biocatalyst for the photoreduction of CO_2/HCO_3^- to formate. The present system is an artificial model that mimics the functions of this biocatalyst.

It should be noted that in the present study a photosystem has been applied to characterize the catalytic activity of the Pd–β-CD colloid only as a matter of convenience. The high quantum efficiency of $MV^{\bullet+}$ generation in these systems provides a rapid and effective accumulation of the electron carrier, $MV^{\bullet+}$, that does not affect or influence the subsequent kinetics of formate production. In fact, any other route that generates $MV^{\bullet+}$ could lead to the catalyzed reduction of HCO_3^- to formate. Indeed, electrogenerated $MV^{\bullet+}$ similarly mediates the reduction of HCO_3^- to formate in the presence of the Pd–β-CD catalyst. Our results reveal that the preparation conditions of the Pd–β-CD tremendously affect the resulting catalytic activities of the colloids. Although the origin of the different activities of Pd–β-CD colloids is not fully understood, we suggest that temperature-controlled morphological differences in the metal colloid clusters are responsible for the different activities. Our results imply that similar Pd catalysts might have potential catalytic activities in hydrogenation or electrochemical reduction of CO_2/HCO_3^-. These aspects, as well as attempts to characterize the activated species of HCO_3^- and HCO_2^- on the Pd–β-Cd catalyst, are now being further examined in our laboratory.

Acknowledgment. This research is supported by a grant from the National Council for Research and Development, Israel, and the Kernforschung Anlage, Jeulich, Germany, and in part by the Belfer Center for Energy Research, Israel.